NASA Contractor Report 187586
ICASE Report No. 91-49

ICASE

OPTIMAL CONTROL OF LIFT/DRAG RATIO ON A ROTATING CYLINDER

Yuh-Roung Ou
John A. Burns

Contract No. NAS1-18605
June 1991

Institute for Computer Applications in Science and Engineering
NASA Langley Research Center
Hampton, Virginia 23665-5225

Operated by the Universities Space Research Association

National Aeronautics and
Space Administration

Langley Research Center
Hampton, Virginia 23665-5225

Optimal Control of Lift/Drag Ratios on a Rotating Cylinder

Yuh-Roung Ou[1]
Institute for Computer Applications in Science and Engineering
NASA-Langley Research Center
Hampton, VA 23665

and

John A. Burns[2]
Interdisciplinary Center for Applied Mathematics
Department of Mathematics
Virginia Polytechnic Institute and State University
Blacksburg, VA 24061

ABSTRACT

We present the numerical solution to a problem of maximizing the lift to drag ratio by rotating a circular cylinder in a two-dimensional viscous incompressible flow. This problem is viewed as a test case for the newly developing theoretical and computational methods for control of fluid dynamic systems. We show that the time averaged lift to drag ratio for a fixed finite-time interval achieves its maximum value at an optimal rotation rate that depends on the time interval.

[1]This research was supported by the National Aeronautics and Space Administration under NASA Contract No. NAS1-18605 and the Air Force Office of Scientific Research under AFOSR Grant No. 89-0079 while the author was in residence at the Institute for Computer Application in Science and Engineering (ICASE), NASA Langley Research Center, Hampton, VA 23665.

[2]This work was supported in part by AFOSR under grant AFOSR-89-0001 and by the National Aeronautics and Space Administration under Contract No. NAS1-18605 while the author was in residence at the Institute for Computer Application in Science and Engineering (ICASE), NASA Langley Research Center, Hampton, VA 23665.

1. INTRODUCTION

Active control of fluid dynamic systems is an area of research that has been considerable growth during the past ten years. This activity is motivated by several potential applications in engineering sciences and optimal design. The development of theoretical frameworks and the construction of practical computational algorithms for control design are highly complex problems. In this paper we consider the problem of maximizing lift to drag ratio by rotating a circular cylinder. This problem is simple enough to be solved by direct numerical calculation (as we do here) and complex enough to serve as an excellent test problem for future theoretical and computational approaches. The main objective of this short note is to provide the solution to two optimization problems that can be used as test examples by researchers in this area.

2. MATHEMATICAL FORMULATION AND NUMERICAL METHOD

In this paper we consider an optimal control problem for a two-dimensional viscous incompressible flow generated by a circular cylinder started impulsively into a combined steady rotatory and rectilinear motion. This problem is investigated numerically by solving a velocity/vorticity formulation of the Navier-Stokes equations [2, 4]. A nonrotating reference frame translating with the cylinder is employed, and the cylinder rotates in the counterclockwise direction with angular velocity $\vec{\Omega}$. The Reynolds number $Re = 2Ua/\nu$ is based on the cylinder diameter $2a$ and the magnitude U of the rectilinear velocity. The angular/rectilinear speed ratio $\alpha = \Omega a/U$ is the primary control parameter in this paper. The speed ratio α can impose significant influences on the characteristics of resulting flow field as well as the temporal evolution of forces on the cylinder surface.

In this formulation, the dimensionless governing equations consist of the vorticity transport equation

$$\frac{\partial \omega}{\partial t} + \vec{u} \cdot \nabla \omega = \frac{2}{Re} \nabla^2 \omega \tag{1}$$

and the vector Poisson equation for the velocity

$$\nabla^2 \vec{u} = -\nabla \times (\omega \vec{e_z}). \tag{2}$$

The cylinder radius a is used as the length scale while a/U is used as the time scale. The dimensionless boundary conditions for the problem of a rotating cylinder are

$$\begin{cases} \vec{u} = -\alpha \sin\theta \vec{e_x} + \alpha \cos\theta \vec{e_y} & \text{on the cylinder surface} \\ \vec{u} = \vec{e_x} & \text{at infinity.} \end{cases} \tag{3}$$

This velocity/vorticity formulation is especially well suited to treating initial development of the flow generated by impulsively started bodies, in which the flow field is composed of a relatively small vortical viscous region embedded in a much larger inviscid potential flow. Consequently, the computational domain may be restricted to a smaller region where the vorticity contributions are contained.

The vorticity transport equation (1) is first discretized by a second order central difference in the radial direction and a pseudospectral transform method in the circumferential direction for all spatial derivatives. This semi-discretization form of equation (1), consisting of a system of ordinary differential equations in time can be written as

$$\frac{d\hat{\omega}}{dt} = F(\hat{\omega}), \quad \hat{\omega} = (\omega_{2,2}, \cdots, \omega_{M-1,N-1})^T, \tag{4}$$

for all the interior grid points. Therefore, the calculation procedure consists of the following steps to advance the solution for any given time increment:

Step 1: Internal vorticity over the fluid region at each interior field point is calculated by solving the discretized vorticity transport equation. An explicit second-order rational Runge-Kutta marching scheme based on the work of [8] is used to advance in time for (4).

The discretization in time of (4) thus can be written as

$$\hat{\omega}^{n+1} = \hat{\omega}^n + \frac{2\hat{g_1}(\hat{g_1}, \hat{g_3}) - \hat{g_3}(\hat{g_1}, \hat{g_1})}{(\hat{g_3}, \hat{g_3})} \tag{5}$$

with

$$\hat{g_1} = F(\hat{\omega}^n)\Delta t,$$

$$\hat{g}_2 = F(\hat{\omega}^n + 0.5\hat{g}_1)\Delta t, \tag{6}$$

$$\hat{g}_3 = 2\hat{g}_1 - \hat{g}_2,$$

where $(\hat{g}_1, \hat{g}_3)$ denotes the scalar product of $\hat{g}_1$ and $\hat{g}_3$. This step consists of the kinetic part of the computational loop.

Step 2: Using known internal vorticity values at all the interior grid points from step 1, the generalized Biot-Savart law of induced velocity

$$\vec{u}(\vec{r_b}, t) = -\frac{1}{2\pi}\int\int_D \frac{\vec{\omega}(\vec{r}, t) \times (\vec{r} - \vec{r_b})}{|\vec{r} - \vec{r_b}|^2} dA$$
$$-\frac{1}{2\pi}\int\int_B \frac{2\vec{\Omega}(\vec{r}, t) \times (\vec{r} - \vec{r_b})}{|\vec{r} - \vec{r_b}|^2} dA + \vec{U} \tag{7}$$

is used to update the boundary vorticity values at all the surface nodes. Here $\vec{r_b}$ represent all grid points located on the solid boundary.

One of difficulties encountered in the simulation of viscous flow is to prescribe the appropriate nonvelocity boundary conditions at the solid surface. The boundary vorticity is required for the formulation based on the velocity/vorticity (or stream-function/vorticity) variables. In order to overcome this particular difficulty, we pose the kinematic relationship between velocity and vorticity fields on the infinite domain in the integral form of (7). This boundary integral method proposed by Wu and Thompson [9] provides the basic link between the velocity and vorticity fields throughout the numerical computations.

Step 3: At this stage, all the vorticity values in the computational domain are known at the new time level. Then, the velocity at points on the outer perimeter of the computational domain is calculated by this integral kinematic constraint

$$\vec{u}(\vec{r_0}, t) = -\frac{1}{2\pi}\int\int_D \frac{\vec{\omega}(\vec{r}, t) \times (\vec{r} - \vec{r_0})}{|\vec{r} - \vec{r_0}|^2} dA$$
$$-\frac{1}{2\pi}\int\int_B \frac{2\vec{\Omega}(\vec{r}, t) \times (\vec{r} - \vec{r_0})}{|\vec{r} - \vec{r_0}|^2} dA + \vec{U}. \tag{8}$$

Here $\vec{r_0}$ denotes the points located on the outer perimeter of the computational domain.

In fact, this integral representation allows us to determine the velocity point-by-point explicitly if all vorticity values are known everywhere in the domain of interest. Moreover,

it often exhibits more realistic behavior at the outer perimeter of the computational domain than asymptotic techniques used in other formulations [1]. This indicates that the difficulty resulting from the imposed far-field condition is removed by the application of this integral constraint.

Step 4: The new velocity field can be established by solving the Poisson equations (2) with prescribed solid boundary conditions and outer boundary conditions that have been determined from step 3.

The final form of the discretized Poisson equations can be written

$$\begin{cases} \mathbf{A}\mathbf{u} = \mathbf{f_1} \\ \mathbf{A}\mathbf{v} = \mathbf{f_2}, \end{cases} \tag{9}$$

where $\mathbf{u}$ and $\mathbf{v}$ are the vectors of unknown interior nodal values. The resulting 11-banded matrix equations are then solved by a preconditioned biconjugate gradient routine [3]. This step completes the computational loop for each time level.

One further important point to be noted in the boundary integral approach is the determination of the initial flow field. In contrast to the special technique used by Badr & Dennis [1], this integral approach enables the numerical code to generate the initial velocity field by executing one cycle of the solution procedure (from step 2 to step 4) rather than employing any additional treatments.

3. RESULTS AND DISCUSSIONS

To assess the numerical algorithm, calculations were performed over a wide range of angular/rectilinear speed ratio α up to 3.25 at a Reynolds number of 200. In this model, the rectilinear velocity is fixed as a constant value while the angular velocity is treated as a control variable. Although the angular velocity can be time-dependent, in this paper angular velocity has been restricted to the constant values. For the works of a rotating cylinder undergoing various kind of time-dependent rotation rate (which include time-harmonic rotatory oscillations and time-periodic rotations with different angular amplitudes and frequencies), the reader is referred to Ou [6] and in the forthcoming paper [7].

We have tested the model against the experimental work of Coutanceau & Ménard [5] with excellent agreement. Selected instantaneous streamline plots for constant value of speed ratio at $\alpha = 2.07$ are presented in figures 1(a,b). We note that for higher values of α vortex shedding continues to occur as a result of cylinder rotation [4]. However, the formation of the vortex street behind the rotating cylinder at high α ($\alpha = 3.25$) is not observed in the experiments of Coutanceau & Ménard. The experiments were unable to detect this vortex shedding because of the length limitation of the water tank and the flow visualization techniques used in their work [5].

The lift and drag coefficients can be calculated in r-θ coordinates as

$$C_L = \frac{2}{Re}\int_0^{2\pi}\left[-\left(\frac{\partial\omega}{\partial r}\right)_b + \omega_b\right]\cos\theta d\theta \tag{10}$$

and

$$C_D = \frac{2}{Re}\int_0^{2\pi}\left[\left(\frac{\partial\omega}{\partial r}\right)_b - \omega_b\right]\sin\theta d\theta, \tag{11}$$

where the subscript b denotes quantities evaluated on the cylinder surface. In particular, we denote the positive values of C_L in the $-y$ direction. The effect of the speed ratio ($0 < \alpha \leq 3.25$) on the temporal evolution of lift/drag coefficient is shown in Figures 2. Note that the lift/drag increment is manifested timewise for the speed ratio up to $\alpha = 2.07$. However, it does not imply that as the speed ratio further increases, the flow field will result in a further improvement of lift and reduction of drag on the cylinder. On the contrary, the adverse effect of speed ratio on the lift/drag is quite evident if a comparison is made between $\alpha = 3.25$ and $\alpha = 2.07$. Notice that for all α less than 2, in the initial time interval, the slope of the lift/drag curve seems to increase with increasing of α. When α becomes greater than 2, the slopes decrease gradually as α increases. For all speed ratios considered here, a significant increase in $(C_L/C_D)_{max}$ is obtained with increment of α. However, (C_L/C_D) achieves its maximum value at much later time for a higher α. We are interested in the problem of maximizing the averaged (C_L/C_D) on a fixed finite time interval.

Figure 3 shows the effect of the speed ratio on time-average (for $0 \leq t \leq 24$) lift, drag and lift/drag coefficients in the range of $0 < \alpha \leq 3.25$. It illustrates that the lift

average is almost linearly proportional to the speed ratio. On the other hand, the drag average remains almost constant up to $\alpha = 2$, then monotonically increases with speed ratio thereafter. Consequently, the resulting lift/drag average is *not* linearly proportional to the speed ratio α. Moreover, the maximum lift/drag average occurs approximately at $\alpha = 2.38$, and it represents a substantial increase of 440% with respect to $\alpha = 0.5$.

It is also of interest to study effect of speed ratio on the variation of the (total lift)/(total drag) force ratio. As shown in Figure 4 this ratio is similar to the lift/drag average in Figure 3 and achieves its maximum value between $\alpha = 2.0$ and $\alpha = 2.38$.

4. CONCLUSIONS

We have presented numerical solutions of two "flow control problems". The first problem is to find α_1^* that maximizes the time-averaged lift to drag functional

$$\mathcal{J}_1(\alpha) = \frac{1}{24}\int_0^{24}\left[\frac{C_L(t,\alpha)}{C_D(t,\alpha)}\right]dt,$$

and the second problem is to find α_2^* that maximizes the total lift to total drag functional

$$\mathcal{J}_2(\alpha) = \frac{\int_0^{24} C_L(t,\alpha)dt}{\int_0^{24} C_D(t,\alpha)dt}.$$

Based on a velocity/vorticity formulation of the Navier-Stokes equations, a finite-difference scheme was used to directly calculate $\mathcal{J}_1(\alpha)$ and $\mathcal{J}_2(\alpha)$ for $0 < \alpha \leq 3.25$. It is hoped that these solutions will useful as base line values for comparison with other approaches to these problems.

Acknowledgments

The authors gratefully acknowledge Dr. Yeng-Ming Chen for many valuable discussions during initial stage of this work. Thanks are also due to Dr. M. Coutanceau for providing the experimental results.

References

[1] H. M. Badr and S. C. R. Dennis, Time-dependent viscous flow past an impulsively started rotating and translating circular cylinder, *J. Fluid Mech.* **158**, 447-488 (1985).

[2] Y.-M. Chen, *Numerical simulation of the unsteady two-dimensional flow in a time-dependent doubly-connected domain*, phD thesis, University of Arizona, (1989).

[3] Y.-M. Chen, A. E. Koniges and D. V. Anderson, ILUBCG2-11: Solution of 11-banded nonsymmetric linear equation systems by a preconditioned biconjugate gradient routine, *Comp. Phys. Comm.* **55**, 359-365 (1989).

[4] Y.-M. Chen, Y.-R. Ou and A. J. Pearlstein, Development of the wake behind a circular cylinder impulsively started into rotatory and rectilinear motion: intermediate rotation rates, ICASE Report 91-10, submitted to J. Fluid Mech. (1991).

[5] M. Coutanceau and C. Ménard, Influence of rotation on the near-wake development behind an impulsively started circular cylinder, *J. Fluid Mech.* **158**, 399-446 (1985).

[6] Y.-R. Ou, Active control of flow around a rotating cylinder, In *Meeting on Turbulence Structure and Control*, Cosponsored by AFOSR and Ohio State University, Columbus, April 1-3, (1991).

[7] Y.-R. Ou and J. A. Burns, Effect of rotation rate on the forces of a rotating cylinder, ICASE Report in preparation, (1991).

[8] A. Wambecq, Rational Runge-kutta methods for solving systems of ordinary differential equations, *Computing* **20**, 333-342 (1978).

[9] J. C. Wu and J. F. Thompson, Numerical solutions of time-dependent incompressible Navier-Stokes equations using an integral-differential formulation, *Computers & Fluids* **1**, 197-215 (1973).

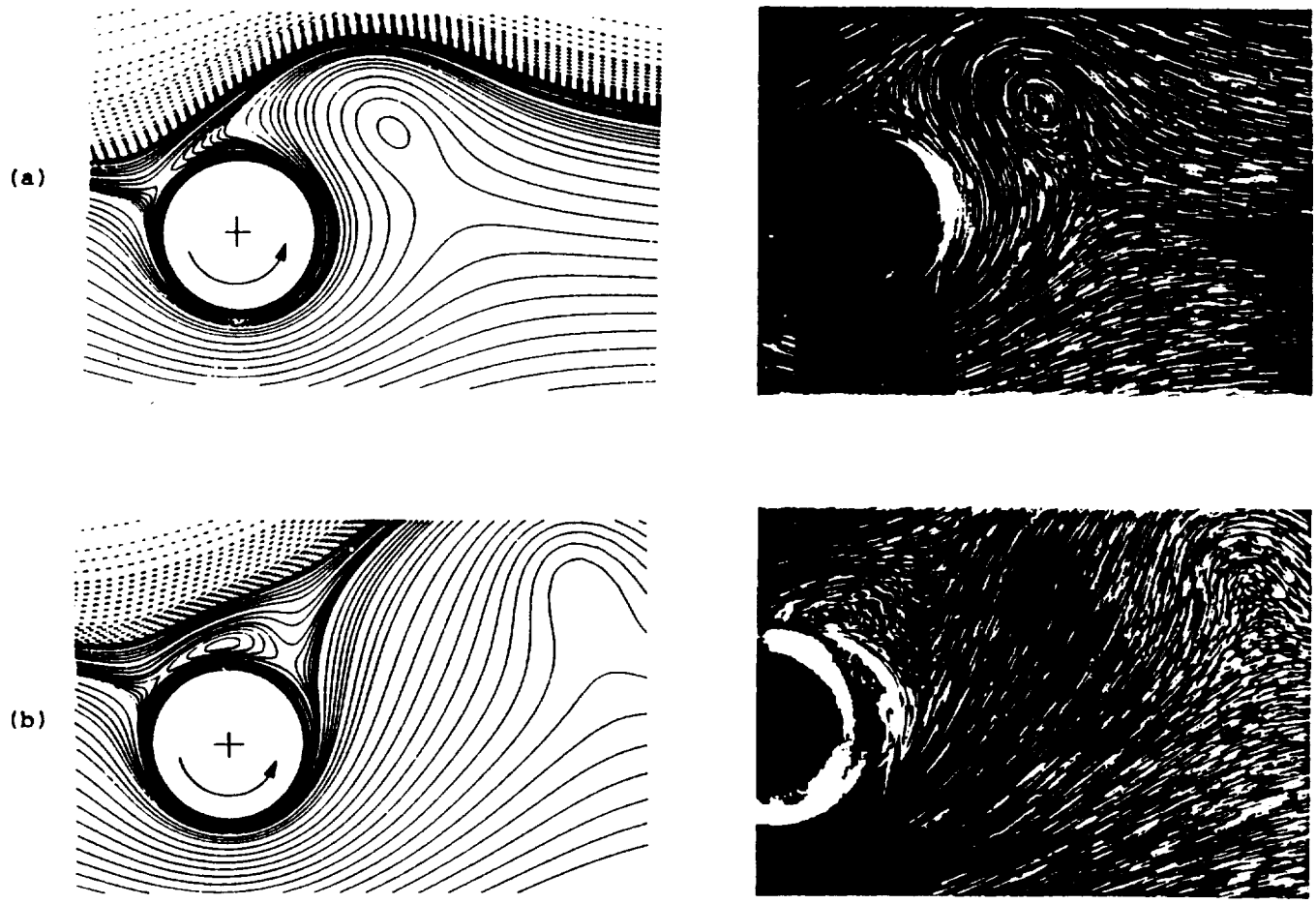

Figure 1. Comparison of calculated (left) and experimental (right) instantaneous streamlines for Re = 200, α = 2.07. (a) t = 5.0, (b) t = 9.0.

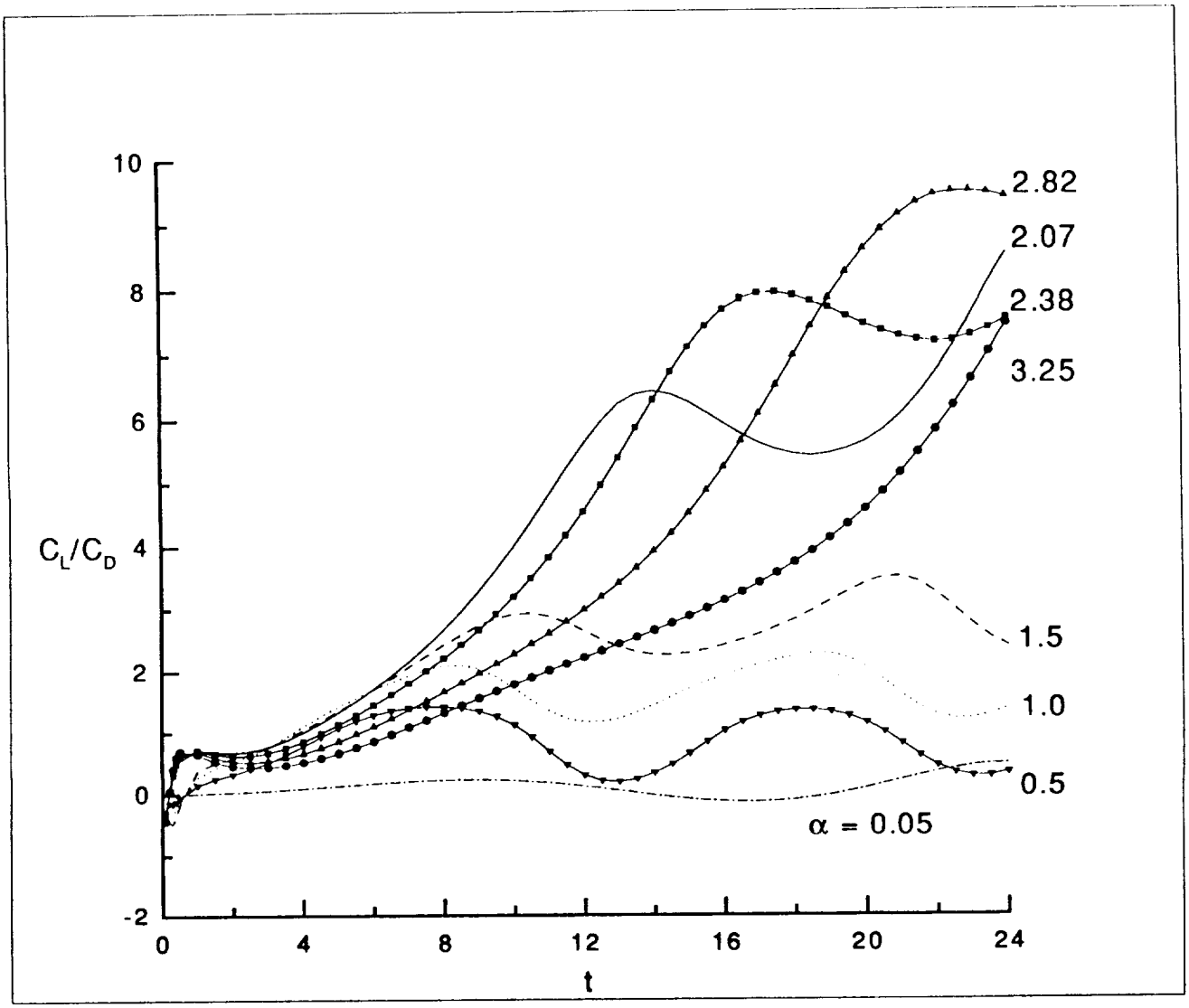

Figure 2. Temporal evolution of the lift/drag coefficient at various values of speed ratio ($0 < \alpha \leq 3.25$) up to $t = 24.0$.

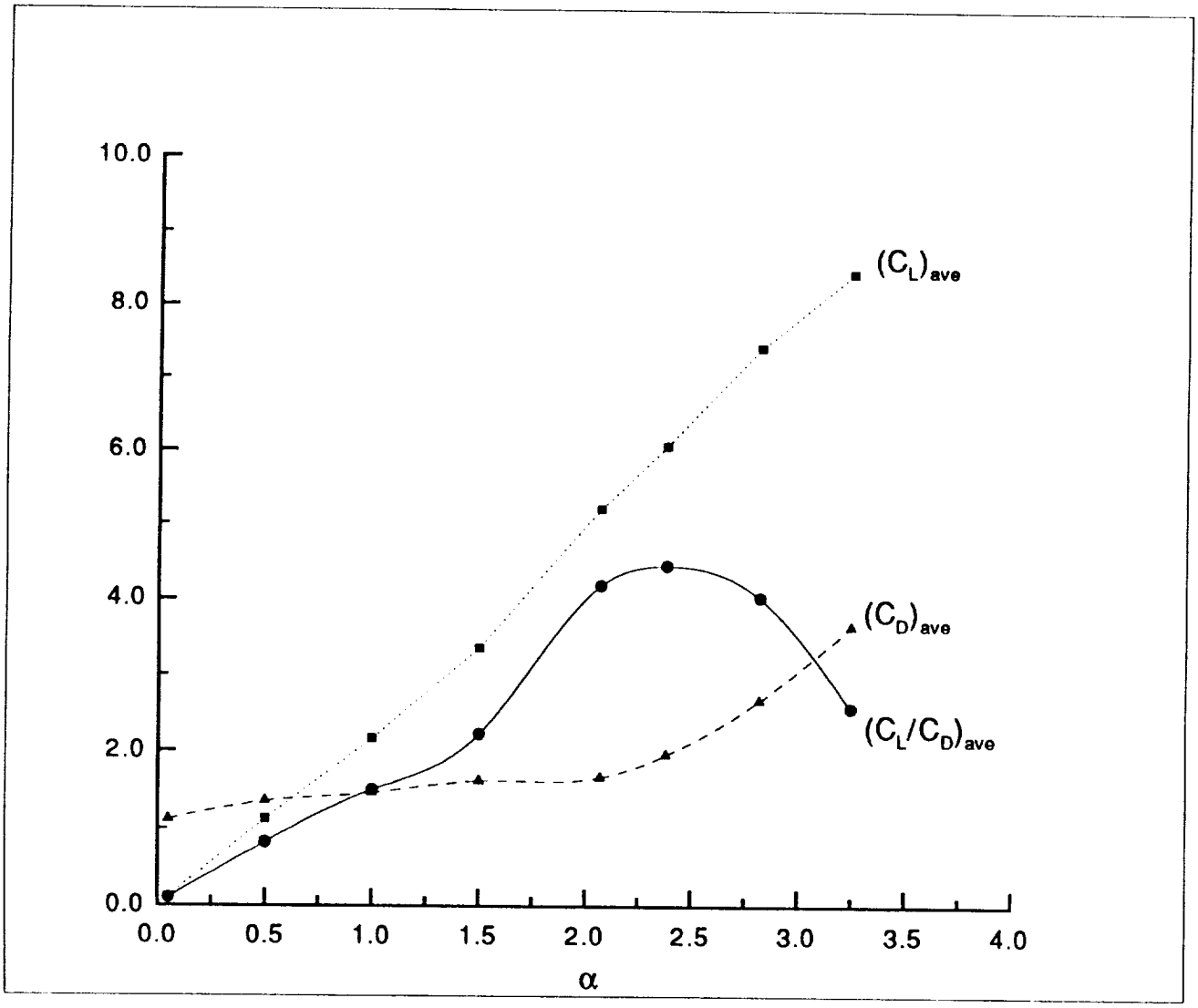

Figure 3. Effect of speed ratio on time-average lift, drag and lift/drag coefficients for $0 < \alpha \leq 3.25$.

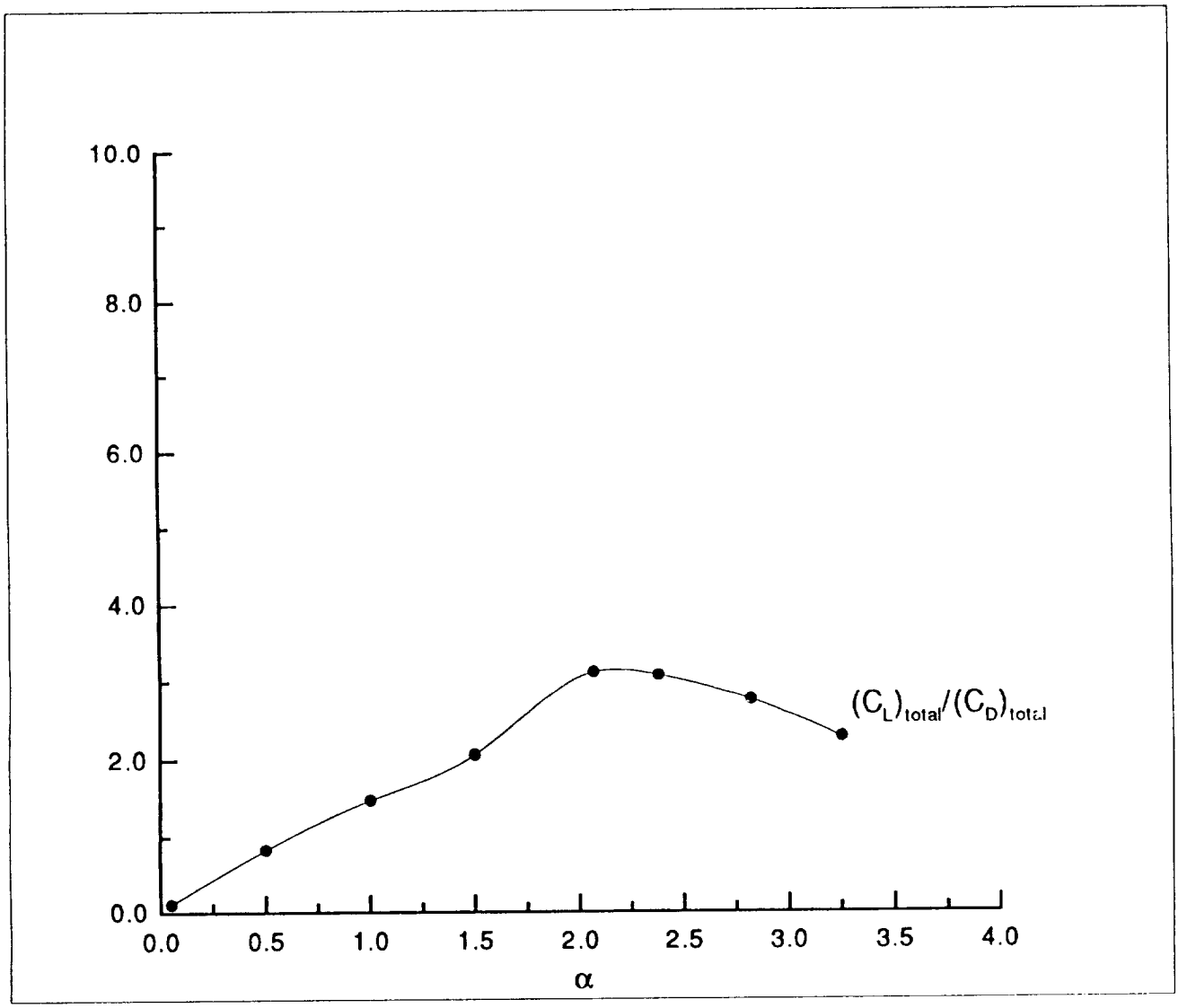

Figure 4. Effect of speed ratio on variation of total lift/total drag force ratio.

Report Documentation Page

1. Report No.	2. Government Accession No.	3. Recipient's Catalog No.
NASA CR-187586 ICASE Report No. 91-49		

4. Title and Subtitle	5. Report Date
OPTIMAL CONTROL OF LIFT/DRAG RATIO ON A ROTATING CYLINDER	June 1991
	6. Performing Organization Code

7. Author(s)	8. Performing Organization Report No.
Yuh-Roung Ou John A. Burns	91-49
	10. Work Unit No.
	505-90-52-01

9. Performing Organization Name and Address	11. Contract or Grant No.
Institute for Computer Applications in Science and Engineering Mail Stop 132C, NASA Langley Research Center Hampton, VA 23665-5225	NAS1-18605
	13. Type of Report and Period Covered
	Contractor Report

12. Sponsoring Agency Name and Address	14. Sponsoring Agency Code
National Aeronautics and Space Administration Langley Research Center Hampton, VA 23665-5225	

15. Supplementary Notes

Langley Technical Monitor:
Michael F. Card

Submitted to Applied Mathematics Letters

Final Report

16. Abstract

We present the numerical solution to a problem of maximizing the lift to drag ratio by rotating a circular cylinder in a two-dimensional viscous incompressible flow. This problem is viewed as a test case for the newly developing theoretical and computational methods for control of fluid dynamic systems. We show that the time averaged lift to drag ratio for a fixed finite-time interval achieves its maximum value at an optimal rotation rate that depends on the time interval.

17. Key Words (Suggested by Author(s))	18. Distribution Statement
lift-to-drag ratio, flow control	34 - Fluid Mechanics and Heat Transfer 63 - Cybernetics Unclassified - Unlimited

19. Security Classif. (of this report)	20. Security Classif. (of this page)	21. No. of pages	22. Price
Unclassified	Unclassified	13	A03

NASA FORM 1626 OCT 86

NASA-Langley, 1991